JACS
JOURNAL OF THE AMERICAN CHEMICAL SOCIETY

ARTICLE

pubs.acs.org/JACS

Nanospheres of a New Intermetallic $FeSn_5$ Phase: Synthesis, Magnetic Properties and Anode Performance in Li-ion Batteries

Xiao-Liang Wang,[†] Mikhail Feygenson,[‡,§] Haiyan Chen,[∥] Chia-Hui Lin,[‡] Wei Ku,[‡] Jianming Bai,[⊥,#] Meigan C. Aronson,[‡,§] Trevor A. Tyson,[∥] and Wei-Qiang Han*[,†]

[†]Center for Functional Nanomaterials and [‡]Condensed Matter Physics and Materials Science Department, Brookhaven National Laboratory, Upton, New York 11973, United States

[§]Department of Physics and Astronomy, Stony Brook University, Stony Brook, New York 11794, United States

[∥]Physics Department, New Jersey Institute of Technology, Newark, New Jersey 07102, United States

[⊥]Materials Science and Engineering, University of Tennessee, Knoxville, Tennessee 37996, United States

[#]High Temperature Materials Laboratory, Oak Ridge National Laboratory, Oak Ridge, Tennessee 37831, United States

ABSTRACT: We synthesized monodisperse nanospheres of an intermetallic $FeSn_5$ phase via a nanocrystal-conversion protocol using preformed Sn nanospheres as templates. This tetragonal phase in *P*4/*mcc* space group, along with the defect structure $Fe_{0.74}Sn_5$ of our nanospheres, has been resolved by synchrotron X-ray diffraction and Rietveld refinement. Importantly, $FeSn_5$, which is not yet established in the Fe−Sn phase diagram, exhibits a quasi-one dimensional crystal structure along the *c*-axis, thus leading to interesting anisotropic thermal expansion and magnetic properties. Magnetization measurements indicate that nanospheres are superparamagnetic above the blocking temperature T_B = 300 K, which is associated with the higher magnetocrystalline anisotropy constant K = 3.33 kJ m^{-3}. The combination of the magnetization measurements and first-principles density functional theory calculations reveals the canted antiferromagnetic nature with significant spin fluctuation in lattice *a*−*b* plane. The low Fe concentration also leads $Fe_{0.74}Sn_5$ to enhanced capacity as an anode in Li ion batteries.

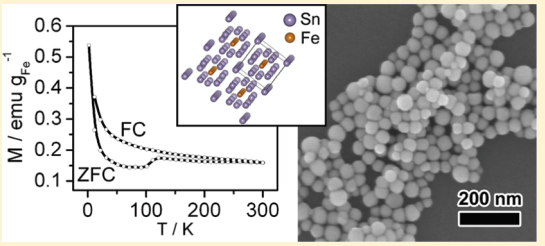

INTRODUCTION

Nanocrystal conversion chemistry is evolving as a powerful general strategy for synthesizing complex solids.[1,2] The concept involves utilizing preformed simple nanostructures as templates to promote compositional and morphological attributes on final products through, for instance, galvanic-replacement reactions and diffusion-based methods.

One good example is the conversion of compositionally simple tin nanocrystals into several complex tin-based intermetallics whose shapes (nanocubes, nanospheres, or nanorods) and sizes are directed by these tin templates.[3] It is fascinating that these intermetallics form so readily by this route, in contrast to bulk systems (e.g., $FeSn_2$ and $CoSn_3$) that are difficult to prepare via conventional high-temperature metallurgy. According to their phase diagrams, these compounds pass through different structures on cooling down from the liquid phase before attaining their ultimate ground states.[4] Instead, this conversion chemistry approach provides a new 'bottom-up' route to synthesize low-temperature phases of intermetallic nanostructures that are otherwise energetically difficult to synthesize. We reproduced the tin intermetallics conversion synthesis and generated M−Sn (M = Fe, Cu, Co, Ni) nanospheres as high-capacity anode materials in Li ion batteries.[5] The second metal M in tin intermetallics is believed to play a key role in enhancing the cell performance by buffering the volume change, stabilizing the integration, and improving the electronic conductivity.[6−8] In practice, the merit of our ability to control both the shape and the size of these nanoparticles by conversion chemistry enables us to compare their intrinsic cell performance and identify the best composition in this important category of tin-based intermetallic electrodes.

Interestingly, during our preparation of the Fe−Sn system, we found that while the $FeSn_2$ phase prevailed over a wide range of the molar ratio of Fe and Sn precursors (i.e., $n(FeCl_3)/n(SnCl_2)$ = 0.3−1), as we lowered it to 0.1, we obtained uniform nanospheres with a new $FeSn_5$ intermetallic phase that was not previously established in the existing Fe−Sn phase diagram. These nanospheres have Fe vacancies and exhibit a single-crystal $Fe_{0.74}Sn_5$/amorphous Fe−Sn−O core−shell nanostructure.

Moreover, the lack of magnetization data in the literature for $FeSn_5$/$FeSn_2$ nanoparticles, combined with the fact that monodisperse single-crystalline nanoparticles may potentially have promise as materials for high-density magnetic recording devices, has motivated us to study the magnetic properties of $Fe_{0.74}Sn_5$ nanospheres and compare it with the known-phase $FeSn_2$ nanospheres.

Received: March 15, 2011
Published: June 16, 2011

We are also interested in its performance as an anode material in Li ion batteries. $FeSn_2$ has been found as the best composition among M−Sn (M = Fe, Cu, Co, Ni) nanospheres.[5] However, the presence of Li storage-inactive Fe in $FeSn_2$ suppresses the theoretical capacity (804 mAh g^{-1}) as compared with pure Sn (993 mAh g^{-1}). $Fe_{0.74}Sn_5$ has a theoretical capacity of 929 mAh g^{-1}, which, to our knowledge, is the highest to date for the demonstrated M−Sn intermetallic anodes, where M is electrochemically inactive.

EXPERIMENTAL SECTION

Chemicals. $SnCl_2$ (anhydrous, 99% min, Alfa), $FeCl_3$ (anhydrous, 97%, Aldrich), polyvinylpyrrolidone (PVP, MW = 360 000, Aldrich), and poly(2-ethyl-2-oxazoline) (PEtOx, MW = 50 000, Alfa) as surface stabilizers; tetraethylene glycol (TEG, 99%, Alfa) as the solvent; and, $NaBH_4$ (98%, Alfa) as the reducing agent.

Synthesis. We obtained the $Fe_{0.74}Sn_5$ nanospheres by two reaction steps in the typical mode of conversion chemistry.[3,9] The first step involved synthesizing templates of uniform tin nanospheres by the reduction of $SnCl_2$ using $NaBH_4$ in TEG; we used PVP and PEtOx as surface stabilizers. In 11.25 mL of TEG, 0.525 g of PVP and 0.225 g of PEtOx were dissolved. Then the solution was heated to 170 °C, and a $SnCl_2$ solution (0.0975 g in 1 mL of TEG) was mixed. After ~10 min, a fresh $NaBH_4$ solution (0.198 g in 6 mL of TEG) was added, drop-by-drop. Tin colloids quickly formed upon the addition, causing the mixture to turn black. The tin template suspensions were stirred at 170 °C for 15 min before we proceeded next to convert them into $Fe_{0.74}Sn_5$ intermetallic nanospheres. To do so, we incorporated an $FeCl_3$ solution (0.008 g in 1 mL of TEG) into the suspension at 170 °C, waited for 10 min, and then held it at 205 °C for 2 h. The synthesis was performed while vigorously stirring the suspension in a three-neck flask filled with argon atmosphere via a Schlenk line. We collected the resulting nanospheres by centrifugation and washed them with ethanol.

Characterization. The X-ray diffraction experiments on the synthesized Fe−Sn samples were carried out on beamline X14A (λ = 0.72958 Å) of the National Synchrotron Light Source (NSLS) at Brookhaven National Laboratory. The diffraction patterns were collected in a Q-range from 0.5 to 8.7 $Å^{-1}$, with a Si strip detector at a 0.005° step size. XRD patterns were analyzed using the software Jade 6.5 (Materials Data Incorporated), Jana 2006 (Petricek, V., Dusek, M., and Palatinus, L., 2006), and Superflip,[10] a program for solving structures using the charge-flipping method.[11] The low-temperature experiments were conducted with a displex cryostat (ADP Cryogenics). The XRD patterns were collected using a Ge (111) analyzing crystal and a point detector at X14A beamline. The lattice parameters were obtained by fitting the XRD data using software TOPAS-Academic V4.1 (Coelho Software, Brisbane, 2007). The wavelength is 0.77599 Å, and the estimated stand deviations for lattice *a* and *c* are 0.0001 Å and 0.0002 Å, respectively.

A Hitachi S-4800 scanning electron microscope (SEM) and a JEM-2100F transmission electron microscope (TEM) with an energy dispersive X-ray spectroscopy (EDS) detector were used for the nanostructural characterization. The EDS measurement was performed in the scanning TEM (STEM) mode with a spot size of 0.7 nm. Differential thermal analysis (DTA) was conducted using a Diamond TG/DTA Instruments (Perkin-Elmer).

To explore the magnetic properties of our new intermetallic nanoparticles, we measured the temperature and field dependencies of the dc magnetization at temperatures from 2 to 300 K and in a magnetic field of 50 kOe, using the Quantum Design magnetic property measurement system (MPMS). For temperatures 300−850 K, we employed a vibrating sample magnetometer in a Quantum Design physical property measurement system (PPMS). We dispersed about 10 mg of nanoparticles in paraffin and contained them in gelatin capsules fastened in plastic straws for immersion into the MPMS. For the high-temperature measurements in PPMS we used a gold foil to contain the sample. We subtracted the diamagnetic signal from the paraffin and the container from the magnetization data. The magnetization was normalized to the total mass of Fe atoms within each sample.

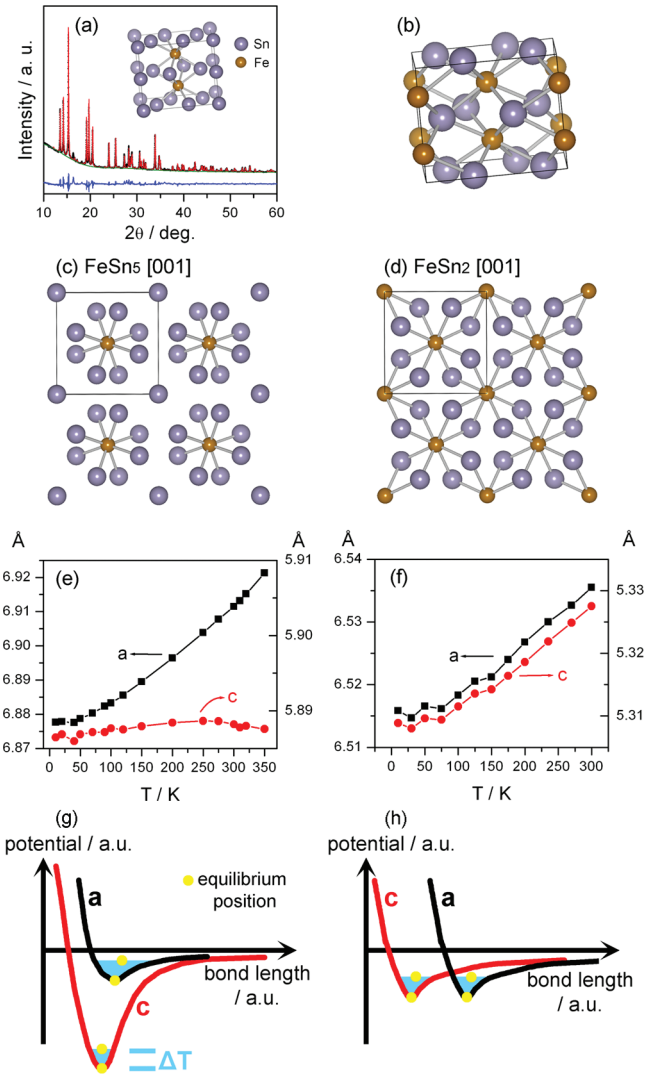

Figure 1. (a) Synchrotron XRD pattern and Rietveld refinement of $Fe_{0.74}Sn_5$. Black dots, observed profile; red line, calculated profile; blue line, difference profile; and olive line, background, with the inset illustrating the crystal structure. (b) The crystal structure of $FeSn_2$, in which the color designation is the same as (a). (c) $Fe_{0.74}Sn_5$ and (d) $FeSn_2$ crystal structures from [001] view direction. (e and f) The variation of lattice constants with temperature, (e) $Fe_{0.74}Sn_5$ and (f) $FeSn_2$. (g and h) The illustration of bond energy diagrams showing the influence of temperature on the thermodynamic equilibrium lattice parameters *a* and *c*, (e) $Fe_{0.74}Sn_5$ and (f) $FeSn_2$.

The electrode films consisted of $Fe_{0.74}Sn_5$ nanospheres, carbon black (Super P Li, TIMCAL), and sodium carboxymethyl cellulose (CMC, MW ~ 90 000, Aldrich) binder with the weight composition of 80:10:10 on copper foils (0.025 mm thick, Schlenk). The composition of $FeSn_2$ electrode was $FeSn_2$ (64 wt %), carbon black (16 wt %), and poly(vinylidene fluoride) binder (PVDF, Alfa, 20 wt %).[5] The electrolyte solution was 1.0 M $LiPF_6$ in ethylene carbonate/dimethyl carbonate (1:1 by volume, Novolyte). The Celgard 2320 membrane served as the separator. We fabricated laminated 2032-type coin cells with an electrode

Table 1. A Calculated Partial Reflection Table Containing the Index, *d* Spacing, and Relative Intensity Information of $Fe_{0.74}Sn_5$

plane index					plane index				
h	*k*	*l*	*d* space, Å	$I_{(211)}$	*h*	*k*	*l*	*d* space, Å	$I_{(211)}$
1	0	0	6.91372	2.2976	4	0	2	1.49062	1.8727
1	1	0	4.88874	3.8671	0	0	4	1.47233	9.0883
2	0	0	3.45686	1.9515	3	1	3	1.46069	12.7922
2	1	0	3.09191	29.0535	4	1	2	1.45713	0.7814
0	0	2	2.94467	43.1326	1	0	4	1.44004	0.1275
2	1	1	2.73757	99.9998	3	3	2	1.42581	0.7464
1	0	2	2.70918	2.0006	1	1	4	1.40979	0.0073
1	1	2	2.52243	3.979	4	3	0	1.38274	4.3444
2	2	0	2.44437	1.4077	5	0	0	1.38274	8.6628
3	0	0	2.30457	1.0547	3	2	3	1.37173	0.2089
2	0	2	2.24163	0.9285	4	2	2	1.36878	4.8223
3	1	0	2.18631	34.3753	5	1	0	1.35589	0.1261
2	1	2	2.13235	47.4433	2	0	4	1.35459	0.0388
3	1	1	2.04963	33.2834	4	3	1	1.34614	6.5926
3	2	0	1.91752	0.9383	2	1	4	1.32931	4.8605
2	2	2	1.8808	0.0795	5	1	1	1.32133	0.0008
3	2	1	1.82331	0.5517	5	2	0	1.28385	0.0214
3	0	2	1.81485	0.3555	4	1	3	1.27501	0.1451
3	1	2	1.75538	18.3496	2	2	4	1.26121	0.2255
4	0	0	1.72843	0.0308	5	2	1	1.25439	1.0263
4	1	0	1.67682	0.0621	5	0	2	1.25162	17.4774
2	1	3	1.65729	23.336	4	3	2	1.25162	11.6573
3	3	0	1.62958	0.0457	3	0	4	1.24074	0.1088
4	1	1	1.61273	0.6462	5	1	2	1.2316	0.1048
3	2	2	1.60686	0.2859	4	4	0	1.22218	0.3474
4	2	0	1.54596	12.0742	3	1	4	1.22123	12.1489
4	2	1	1.4953	19.2061	4	2	3	1.21456	8.9362

film/electrolyte-saturated separator/lithium foil (as the counter and reference electrodes, 0.75 mm thick, 99.9% metal basis, Alfa) inside an M. Braun LabMaster 130 glovebox protected by argon atmosphere. The cycling was performed using an Arbin MSTAT system by a galvanostatic cycling procedure, with the voltage range of 0.05−1.5 V and the current rate of C/20 (i.e., the time for full charge or discharge of the theoretical capacity was 20 h).

RESULTS AND DISCUSSION

The crystal structure was solved from synchrotron powder XRD data using the charge-flipping method, which has been successfully applied to a structural solution from powder XRD data (Figure 1a).[10,11] Briefly, the space group and lattice constants were obtained from the indexing of XRD pattern of synthesized Fe−Sn compound. With these parameters from the indexing, atomic coordinates were determined through structural solution by the charge-flipping method. A Rietveld refinement of the XRD pattern was then performed using the solved structure, during which the lattice parameters, thermal factors, atomic coordinates, and occupancies were allowed to be refined.

Differing from known Fe−Sn phases (including room-temperature FeSn and $FeSn_2$ phases and high-temperature Fe_5Sn_3 and Fe_3Sn_2 phases),[4] this new $FeSn_5$ phase has a tetragonal lattice in the *P*4/*mcc* space group. The lattice parameters of $Fe_{0.74}Sn_5$ were refined as $a = b = 6.91369$ Å, $c = 5.88967$ Å, and $\alpha = \beta = \gamma = 90°$, with a weighted *R*-factor $R_{wp} < 3\%$. The atomic coordinates of the Fe and Sn atoms are as follows: Fe (1/2, 1/2, 1/4), Sn1 (0, 0, 1/2), and Sn2 (0.190, 0.607, 1/2). In addition, the Rietveld refinement of Fe occupancy in our sample also yielded a Sn/Fe molar ratio of 6.8, indicative of the presence of vacancies at Fe sites. This nonstoichiometry is further supported by our findings from scanning transmission electron microscopy-energy dispersive X-ray spectroscopy (STEM-EDS) with a spot size of 0.7 nm, which return a similar Sn/Fe of 7.0. Moreover, the fact that there are not any extra peaks in the XRD pattern suggests that Fe vacancies are disordered. The calculated partial reflection table containing the index, *d*-spacing, and relative intensity information of $Fe_{0.74}Sn_5$ is given in Table 1.

In our present experimental conditions, the pure intermetallic $FeSn_5$ nanoparticles always come with a large number of Fe vacancies. Upon increasing Fe ratio in the precursors, a mixture with few $FeSn_2$ vacancies results. This means the $FeSn_2$ is energetically preferable when excess of Fe available, implying strongly that the $FeSn_5$ structure is only stable in the presence of large numbers of Fe vacancies.

It is interesting to find that the crystal structure of $FeSn_5$ shares a lot of similarities with that of $FeSn_2$. Besides the same tetragonal lattice and similar lattice constants (for $FeSn_2$, $a = b = 6.534$ Å and $c = 5.326$ Å), there is only one Fe position in each structure. In both cases, each Fe atom is surrounded by eight Sn atoms that form an Archimedian square antiprism (cf. Figure 1a−d; for clarity, only the bonds between Fe atoms and nearest Sn atoms are shown); the distances between the Fe and Sn atoms are similar (2.70347 Å for $FeSn_5$ and 2.79582 Å for $FeSn_2$). Moreover, the distances between two nearest Fe atoms d_{Fe-Fe} are both $c/2$, i.e., 2.94484 Å for $FeSn_5$ and 2.66300 Å for $FeSn_2$. Basically, both structures are based on the building block of $FeSn_8$ antiprism: In $FeSn_2$, the antiprisms form a 3D network, while in $FeSn_5$, they form only a one-dimensional (1D) network along the *c*-axis. The structure of $FeSn_5$ is then stabilized by space filling Sn atoms that hold the antiprisms in place. As to be shown below, such a weakly interconnected 1D network naturally leads to strong quasi-1D characteristics in both structural and magnetic properties of this new material, drastically different from the 3D case of $FeSn_2$.

Looking at the two crystal structures, it seems that in $FeSn_5$, if we substitute the eight corner Sn atoms and the four edge Sn atoms on the *c*-axis with eight edge Fe atoms on the *c*-axis (two Fe atoms on one edge), the crystal structure of $FeSn_5$ may evolve into that of $FeSn_2$. The change of the atom number in the unit cell also supports this evolution; there are in total one corner Sn atom and one edge Sn atom (considering the share of atoms among neighboring unit cells) in $FeSn_5$ that are replaced by two edge Fe atoms, which results in four Fe atoms and eight Sn atoms in the new unit cell, i.e., $FeSn_2$. In this sense, $FeSn_5$ probably is one intermediate phase between Sn and $FeSn_2$.

The low-temperature synchrotron XRD experiments unveiled that the $Fe_{0.74}Sn_5$ lattice (also obtained by the same Rietveld refinement) expands, upon warming up, much more along the *a*-axis than along the *c*-axis, as shown in Figure 1e. As a result, the tetragonality (indicated by c/a) increases monotonically with temperature. This is in great contrast to the tetragonal $FeSn_2$ nanosphere system (Figure 1f), in which the *a* and *c* lattice constants expand at similar rates with increasing temperature, with no appreciable change in tetragonality.

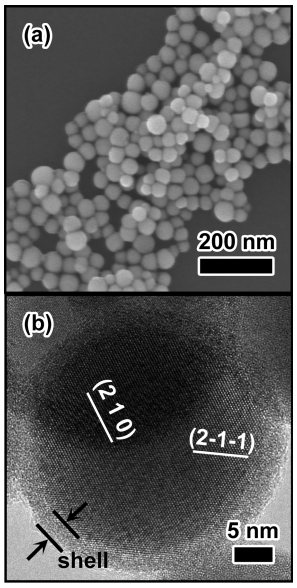

Figure 2. (a) SEM and (b) TEM images of $Fe_{0.74}Sn_5$ nanospheres.

The anisotropic thermal expansion phenomenon has been previously reported in several systems, and one explanation is based on the change in the tilt angle of interpolyhedra in the crystal structures with temperature.[12] The dramatically different behavior in the case of $Fe_{0.74}Sn_5$ as compared with $FeSn_2$, on the other hand, originates from the quasi-1D nature of the structure. Since the bonding between the antiprisms is much weaker than the direct connection within the 1D network along the *c*-axis, the anharmonic regime of the internetwork bonding can be easily reached (thermally) in the *a*−*b* plane, leading to a strong thermal expansion in the plane, as illustrated in Figure 1g and h. This also provides the system additional flexibility to relax without compromising the more robust direct connections within the antiprism along the *c*-axis, leading to a negligible thermal expansion in comparison. Interestingly, a similar anisotropic thermal expansion is observed in $L1_0$ FePt[13] with large magnetic anisotropy energy (MAE),[14] most likely resulting similarly from the very different bonding along the *c*-axis (Fe−Pt layer) and in the *a*−*b* plane (Fe and Pt planes).

$Fe_{0.74}Sn_5$ that we synthesized forms in uniform nanospheres with diameters determined from SEM measurements of 45 ± 9 nm, similar to the tin templates (45 ± 11 nm), as depicted in Figure 2a. The room-temperature densities of tin and this $Fe_{0.74}Sn_5$, respectively, are 7.36 and 7.48 g cm^{-3}. Therefore, a volume expansion of 5% accompanies the conversion of tin into $Fe_{0.74}Sn_5$. The high-resolution transmission electron microscopy (HRTEM) image (Figure 2b) exemplifies the single crystal nature of the $Fe_{0.74}Sn_5$ nanospheres. The ordered atomic arrangement is identical throughout the whole particle, without any indication of grain boundaries. Moreover, the particle is covered by a ∼3 nm amorphous surface layer. The STEM-EDS detection with the spot size of 0.7 nm confirms the existence of Fe, Sn, and O. Therefore, the $Fe_{0.74}Sn_5$ nanospheres possess a core−shell nanostructure built by a single-crystalline intermetallic core and an amorphous Fe−Sn−O oxidized layer. Tin templates also have a similar single crystal core/amorphous shell nanostructure.[9]

The chemical ordering and the tetragonality of FePt alloy have strong influence on its attractive magnetic properties.[15] This makes us interested in studying the magnetic properties of our $Fe_{0.74}Sn_5$, which is characteristic of this quasi-1D structure and the anisotropic thermal expansion.

We have measured the field *H* and temperature *T* dependencies of the magnetization *M* of $Fe_{0.74}Sn_5$ and $FeSn_2$ nanospheres with similar diameters (45 ± 11 nm for $Fe_{0.74}Sn_5$ and 39 ± 7 nm for $FeSn_2$). Powders of nanospheres with both compositions were diluted in paraffin to minimize interparticle interactions for the low-temperature measurements. The magnetization measurements were carried out between 2.0 and 300 K using a Quantum Design MPMS and at higher temperatures 300−1000 K using a vibrating sample magnetometer (VSM) in a Quantum Design PPMS.

The temperature dependencies of *M* for $Fe_{0.74}Sn_5$ and $FeSn_2$ nanoparticles are presented in Figure 3a and b showing the separation below the blocking temperature T_B of the zero field cooled (ZFC) and field cooled (FC) magnetizations that are typical of small magnetic particles when their superparamagnetic fluctuations freeze or that become slower than the measurement time. ZFC and FC magnetizations were measured in an applied field of 500 Oe. The separation of ZFC and FC magnetizations below T_B indicates that there is an energy barrier ΔE proportional to $k_B T_B$ for the reorientation of a net nanoparticle moment that is much larger for $Fe_{0.74}Sn_5$ (T_B∼300 K) than for $FeSn_2$ (T_B∼125 K). Generally, ΔE depends on both the nanoparticle volume *V* and the magnetocrystalline anisotropy *K*, so that $\Delta E \sim KV$. Since the outermost 3 nm of the nanoparticles is amorphous, we will assume that it does not contribute to the nanoparticle magnetization, which is ascribed entirely to the remaining 33 nm diameter core in $FeSn_2$ and 39 nm in $Fe_{0.74}Sn_5$. We estimate that the $Fe_{0.74}Sn_5$ nanospheres have $K = 3.33$ kJ m^{-3}, which is larger than the $K = 2.29$ kJ m^{-3} calculated for the $FeSn_2$ nanospheres. For equal nanoparticle dimensions, it is more difficult to reorient the entire moment of an $Fe_{0.74}Sn_5$ nanoparticle than that of an $FeSn_2$ nanoparticle. The larger anisotropy of $Fe_{0.74}Sn_5$ that is inferred from this measurement likely reflects robust bonding along the *c*-axis but weaker *a*−*b* plane bonding. We note that the values of the magnetocrystalline anisotropy constants of our samples are several magnitudes less than for FePt nanoparticles.[14]

The observation of superparamagnetic behavior implies that each nanoparticle has a net moment. While true long-range order with diverging correlation lengths and time scales cannot be realized in finite sized systems such as nanoparticles, the net nanoparticle moment implies that at least some of the individual moments making up the nanoparticle have fixed relative orientations and are in this sense magnetically ordered below a transition temperature.

We have measured the field dependencies of the magnetization in $Fe_{0.74}Sn_5$ and $FeSn_2$ at 2, 150, and 300 K (Figure 3c and d). In both cases, the magnetization is comprised of two temperature-dependent components. The first is reminiscent of a bulk ferromagnet, being highly nonlinear at low fields and saturating at high fields. A small coercive field of 180 ± 9 Oe is found for $Fe_{0.74}Sn_5$ and a larger value of 750 ± 11 Oe for $FeSn_2$, both at 2 K. The magnitude of this ferromagnetic component of the magnetization shrinks with increasing temperature, vanishing completely above 2 K for $FeSn_2$ but remaining substantial at temperatures at least as large as 300 K for $Fe_{0.74}Sn_5$, which validates our identification of 300 K as the blocking temperature for this sample. The second component of the magnetization is linear in field and is positive for both types of nanoparticles at 2 K and at

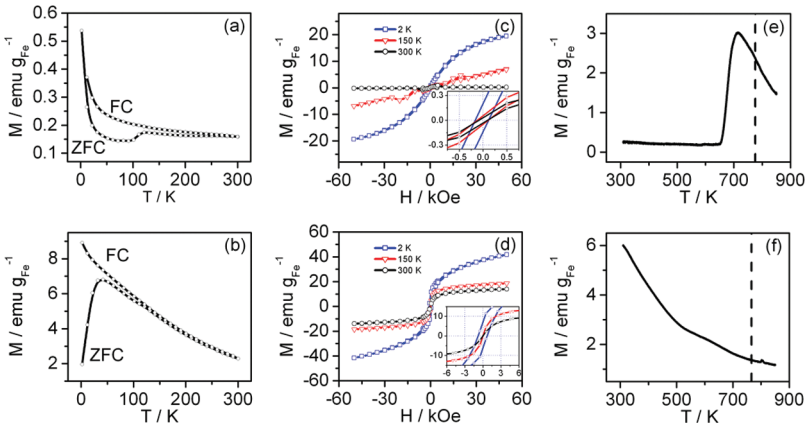

Figure 3. The temperature dependencies of the zero field cooled (ZFC) and field cooled (FC) magnetizations in applied fields of 0.05 kOe for (a) $Fe_{0.74}Sn_5$ and (b) $FeSn_2$ nanospheres. The magnetic field dependencies of the magnetizations for (c) $Fe_{0.74}Sn_5$ and (d) $FeSn_2$ nanospheres, where the insets are expanded views of the same magnetizations but at lower fields. The high-temperature part of the ZFC magnetizations in an applied field of 1 kOe for (e) $Fe_{0.74}Sn_5$ and (f) $FeSn_2$ nanospheres, where the dashed lines indicate the melting points determined from DTA measurements.

higher temperatures becomes much weaker for $FeSn_2$ and $Fe_{0.74}Sn_5$ nanoparticles. This linear magnetization is found in many magnetic nanoparticle systems and is generally ascribed to uncompensated moments that cannot be saturated in field, located perhaps at the particle surface or at the core−shell interface. These uncompensated moments are presumably responsible for the large Curie tail that is evident in both the FC and ZFC $M(T)$ for $Fe_{0.74}Sn_5$ and more weakly in $FeSn_2$, where it is present only in the FC magnetization.

The observation of superparamagnetic behavior in both $Fe_{0.74}Sn_5$ and $FeSn_2$ nanoparticles is definitive proof that some part of each orders at temperatures above 300 K, but it is not a priori evident what the nature of this order is in these multicomponent core−shell particles. For instance, surface atoms are responsible for the paramagnetic contribution in ferri- and ferromagnetic nanoparticles,[16] while in antiferromagnetic nanoparticles, the surface atoms instead are the source of a nonlinear contribution to the magnetization due to a complex magnetic structure with an uneven number of sublattices.[17,18] We have carried out measurements of the magnetization of the $Fe_{0.74}Sn_5$ and $FeSn_2$ nanoparticles above 300 K to search for the onset of long-ranged ferromagnetic or antiferromagnetic order. Since the compound has not been synthesized previously, we have no results from measurements on bulk $FeSn_5$ to constrain this search. DTA shows that the melting temperatures (T_m) of the two compounds are very similar, 776 ± 10 K for $FeSn_2$ and 790 ± 14 K for $Fe_{0.74}Sn_5$. Note that nanoparticles can agglomerate and grow together at temperatures below T_m.

The high-temperature magnetization has very similar properties in the two compounds (Figure 3e and f). It decreases slowly as the temperature is raised above 300 K, and a sharp peak is seen in $Fe_{0.74}Sn_5$ at ∼700 K. We associate this peak with the onset of antiferromagnetic order in the $Fe_{0.74}Sn_5$ cores. There is no overt sign of magnetic order in $M(T)$ for $FeSn_2$, except several slope changes between 450 to 700 K. Since magnetic blocking is observed in $FeSn_2$ and a saturating component of the magnetization is evident at temperatures as large as 300 K, we conclude that $FeSn_2$ orders antiferromagnetically above 300 K. Our measurements have revealed that $Fe_{0.74}Sn_5$ and $FeSn_2$ are mostly likely antiferromagnetic, but that the formation of a moment bearing component via moment canting, sublattice formation, or uncompensated surface moments provides coupling to the external field. We will see below that the theoretical calculations support the presence of antiferromagnetic order in the crystal structures of both $FeSn_2$ and $FeSn_5$.

First-principles density functional theory calculations were carried out to gain additional insight into the magnetic characters of $FeSn_2$ and $Fe_{0.74}Sn_5$. Since our nanoparticles are relatively large, we assume that finite-size effects will provide only small corrections to the bulk electronic structures but not dramatically change the magnetic ground state. We thus calculated the total energy of various magnetic configurations (cf. Table 2 and Figure 4) within the local spin density approximation plus Hubbard U (LSDA+U) approach[19] for three reasonable sets of parameters (U, J) and found consistent qualitative trends for all the parameters sets.

Interestingly, our results in Table 2 show that the lowest energy states in the bulk $FeSn_5$ and $FeSn_2$ are with antiferromagnetic correlation in the plane ($a-b$ plane). $FeSn_2$ is found to have ferromagnetic correlations out of the plane (along c-axis), as previously observed experimentally.[20,21] On the other hand, $FeSn_5$ prefers antiferromagnetic correlation out of the plane. Please see Figure 4c and e for the lowest energy states of $FeSn_5$ and $FeSn_2$, respectively. Also, $FeSn_5$ appears to have much weaker in-plane coupling from the small energy difference between the second and the fourth rows in Table 2. This can be easily understood from the large in-plane Fe−Fe distance in the quasi-1D structure. In other words, for $FeSn_5$, the magnetic structure is hard along c-axis and soft in $a-b$ plane. This is also reminiscent of the hard (i.e., less expansive) c-axis and soft $a-b$ plane during thermal expansion.

These theoretical results support our experimental observations. First, existing experiments on bulk $FeSn_2$ indicate that it is a canted antiferromagnet,[21] and as we explain above, this is likely for the nanoscale version of $FeSn_2$ studied here as well. While there are no measurements of the magnetization of bulk $FeSn_5$, both our theoretical results and measurements on nanoscaled $Fe_{0.74}Sn_5$ support the conclusion that it is also a canted antiferromagnet. Moreover, the relatively weak in-plane coupling of $FeSn_5$ would lead to stronger in-plane spin fluctuations and consequently accounts for the weaker coercive field, larger observed fluctuation

Table 2. For $FeSn_2$ and $FeSn_5$, Calculated Electronic Total Energy of Various Magnetic Configurations and (U, J) in the Scheme of DFT with LSDA+U[a]

		magnetic configurations		electronic total energy, meV		
	lowest energy state	in plane ($a-b$ plane)	out plane (c-axis)	U = 2 eV, J = 0.7 eV	U = 3 eV, J = 0.8 eV	U = 4 eV, J = 0.9 eV
$FeSn_5$		FM	FM	−53.591	−204.294	−409.959
		FM	AF	−130.416	−327.490	−592.195
		AF	FM	−10.150	−146.308	−347.885
	√	AF	AF	−144.855	−348.975	−612.639
$FeSn_2$		FM	FM	−268.073	−392.197	−580.011
		FM	AF	−140.252	−307.907	−525.685
	√	AF	FM	−329.747	−505.486	−711.986
		AF	AF	−226.706	−392.375	−598.877

[a] All the energy values are relative to the non-magnetic configuration. One ferromagnetic and three mostly possible antiferromagnetic orders are chosen in our modeling. FM and AF in this table stand for ferromagnetic and antiferromagnetic, respectively.

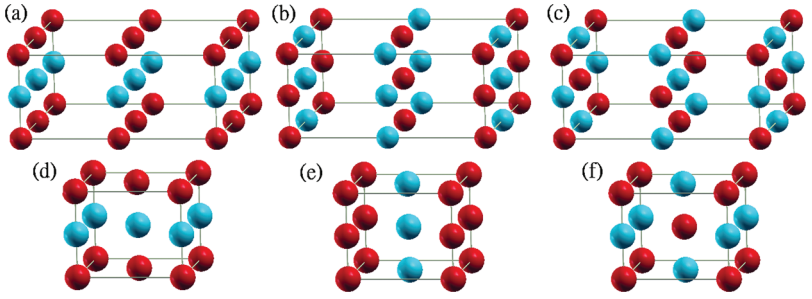

Figure 4. Schematic diagrams of the antiferromagnetic configurations considered in Table 2. Figures (a−c) correspond to the 2nd to 4th rows in Table 2, and (d−f) correspond to the 6th to 8th rows. Only Fe atoms are shown here for simplicity. The box in each diagram is not exactly the chemical unit cell but is meant for better visualization. The vertical axis is the c-axis in their tetragonal lattice. Red and blue Fe atoms carry opposite spins.

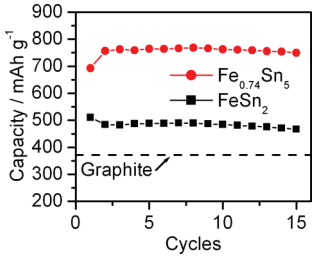

Figure 5. Reversible capacities of $Fe_{0.74}Sn_5$ and $FeSn_2$ nanospheres as anodes in Li ion batteries.

moments, the coexistence of weak ferromagnetic hysteresis and antiferromagnetism, and the disappearance of the nonlinearity in the $M-H$ curve at much lower temperatures.

In our current theoretical scheme, we cannot exclude that the almost one-quarter iron vacancies might change magnetic correlation especially along c-axis (although, the additional electronic scattering resulting from the Fe vacancy is unlikely to favor ferromagnetic coupling). The weaker antiferromagnetic coupling in the $a-b$ plane should be less sensitive to Fe content. More sophisticated theoretical treatment of the vacancies is now on going.

We also studied the cell performance of $Fe_{0.74}Sn_5$ nanospheres as an anode in Li-ion batteries. Its 929 mAh g^{-1} theoretical capacity is the highest to date for the reported M (electrochemically inactive)−Sn intermetallic anodes (the next one is the 852 mAh g^{-1} for $CoSn_3$),[5,22] and is higher than most of the reported systems, where M is active (with exception of Mg_2Sn where Mg can form the solid solution with Li in Mg atomic percentage between 0 and ∼70%).[23,24] $NaSn_6$ (962 mAh g^{-1}, inactive), K_4Sn_{23} (940 mAh g^{-1}, inactive), and $CaSn_3$ (1028 mAh g^{-1}, active) have higher theoretical capacities, but their application as anode materials has not yet been verified.

Because of the low (yet sufficient) Fe concentration, a higher capacity of $Fe_{0.74}Sn_5$ has been achieved as compared with that of $FeSn_2$. As shown in Figure 5, the value stabilizes at around 750 mAh g^{-1} for 15 cycles, while it is around 500 mAh g^{-1} in the case of $FeSn_2$.[5] The initial Coulomb efficiency also increases to 72% for $Fe_{0.74}Sn_5$ from 50% for $FeSn_2$. If we consider the suppression of capacity due to the presence of surface oxidized layer (EDS analysis indicates that the Sn mass percentages in the nanospheres are 89.1% and 75.2% for $Fe_{0.74}Sn_5$ and $FeSn_2$, respectively) and assume that Sn in this layer is active,[25] then the theoretical capacities of these nanospheres become respective 886 mAh g^{-1} ($Fe_{0.74}Sn_5$) and 747 mAh g^{-1} ($FeSn_2$). Therefore, $Fe_{0.74}Sn_5$ nanospheres can achieve 85% of its theoretical capacity, but $FeSn_2$ can realize only 67%.

CONCLUSION

In conclusion, we synthesized nanospheres of a new intermetallic $FeSn_5$ phase by converting preformed Sn nanosphere templates. The nanospheres show a single crystal $Fe_{0.74}Sn_5$/amorphous Fe−Sn−O core−shell structure. $FeSn_5$ has an interesting quasi-1D crystal structure and may serve as one intermediate

phase between Sn and $FeSn_2$. The thermal expansion of the lattice constants of $Fe_{0.74}Sn_5$ nanospheres is highly anisotropic. The magnetization measurements indicated that the blocking temperature (T_B) of the nanospheres is as high as 300 K, due to their high magnetocrystalline anisotropy constants. Moreover, magnetization measurements suggest that the magnetic state of the $Fe_{0.74}Sn_5$ nanospheres is best described as a canted antiferromagnet, which is in agreement with theoretical calculations. Theoretical calculations indicated that the lowest energy state is antiferromagnetic both in $a-b$ plane and along c-axis and confirmed that $FeSn_5$ has rather weak in-plane magnetic coupling. Both the expansion anisotropy and the magnetic properties are attributed to the $FeSn_5$ quasi-1D structure with the strong c-axis and weak $a-b$ plane bondings. Moreover, lowering the Fe concentration is effective in enhancing the cell performance of Fe−Sn intermetallic anodes in Li ion batteries.

AUTHOR INFORMATION

Corresponding Author
whan@bnl.gov

ACKNOWLEDGMENT

This research was carried out at the Center for Functional Nanomaterials (X.L.W. and W.Q.H.), and in the Condensed Matter Physics and Materials Science Department (M.F.,M.C.A., W.K., and J.B.) at Brookhaven National Laboratory (B.N.L.), which are supported by the U.S. Department of Energy, Office of Basic Energy Sciences. This work is supported by the U.S. Department of Energy under contract DE-AC02-98CH10886 and E-LDRD Fund of Brookhaven National Laboratory (X.L.W. and W.Q.H.). Research at the National Synchrotron Light Source X14A beamline was partially sponsored by the U.S. Department of Energy, Office of Energy Efficiency and Renewable Energy, Vehicle Technologies Program, through the Oak Ridge National Laboratory's High Temperature Materials Laboratory User Program and by the Scientific User Facilities Division, Office of Basic Energy Sciences, U.S. Department of Energy.

REFERENCES

(1) Vasquez, Y.; Henkes, A. E.; Bauer, J. C.; Schaak, R. E. *J. Solid State Chem.* **2008**, *181*, 1509–1523.
(2) Yin, Y. D.; Rioux, R. M.; Erdonmez, C. K.; Hughes, S.; Somorjai, G. A.; Alivisatos, A. P. *Science* **2004**, *304*, 711–714.
(3) Chou, N. H.; Schaak, R. E. *J. Am. Chem. Soc.* **2007**, *129*, 7339–7345.
(4) Okamoto, H. *Desk handbook: Phase diagrams for binary alloys*. ASM International: Materials Park, OH, 2000.
(5) Wang, X. L.; Han, W. Q.; Chen, J. J.; Graetz, J. *ACS Appl. Mater. Interfaces* **2010**, *2*, 1548–1551.
(6) Mao, O.; Dahn, J. R. *J. Electrochem. Soc.* **1999**, *146*, 414–422.
(7) Kepler, K. D.; Vaughey, J. T.; Thackeray, M. M. *Electrochem. Solid-State Lett.* **1999**, *2*, 307–309.
(8) Tarascon, J. M.; Armand, M. *Nature* **2001**, *414*, 359–367.
(9) Wang, X. L.; Feygenson, M.; Aronson, M. C.; Han, W. Q. *J. Phys. Chem. C* **2010**, *114*, 14697–14703.
(10) Palatinus, L.; Chapuis, G. *J. Appl. Crystallogr.* **2007**, *40*, 786–790.
(11) Oszlanyi, G.; Suto, A. *Acta Crystallogr., Sect. A* **2004**, *60*, 134–141.
(12) Achary, S. N.; Chakraborty, K. R.; Patwe, S. J.; Shinde, A. B.; Krishna, P. S. R.; Tyagi, A. K. *Mater. Res. Bull.* **2006**, *41*, 674–682.
(13) Tsunoda, Y.; Kobayashi, H. *J. Magn. Magn. Mater.* **2004**, *272−276*, 776–777.
(14) Skomski, R.; Coey, J. M. D. *Permanent Magnetism*. Institute of Physics Publishing: London, U.K., 1999.
(15) Lyubina, J.; Opahle, I.; Muller, K. H.; Gutfleisch, O.; Richter, M.; Wolf, M.; Schultz, L. *J. Phys.: Condens. Matter* **2005**, *17*, 4157–4170.
(16) Coey, J. M. D. *Phys. Rev. Lett.* **1971**, *27*, 1140–1142.
(17) Zhang, W. S.; Bruck, E.; Zhang, Z. D.; Tegus, O.; Li, W. F.; Si, P. Z.; Geng, D. Y.; Buschow, K. H. J. *Physica B* **2005**, *358*, 332–338.
(18) Feygenson, M.; Kou, A.; Kreno, L. E.; Tiano, A. L.; Patete, J. M.; Zhang, F.; Kim, M. S.; Solovyov, V.; Wong, S. S.; Aronson, M. C. *Phys. Rev. B* **2010**, *81*, 014420.
(19) Anisimov, V. I.; Aryasetiawan, F.; Lichtenstein, A. I. *J. Phys.: Condens. Matter* **1997**, *9*, 767–808.
(20) Iyengar, P. K.; Dasannacharya, B. A.; Vijayaraghavan, P. R.; Roy, A. P. *J. Phys. Soc. Jpn.* **1962**, *17*, 247–248.
(21) Lecaer, G.; Malaman, B.; Venturini, G.; Fruchart, D.; Roques, B. *J. Phys. F: Met. Phys.* **1985**, *15*, 1813–1827.
(22) Alcantara, R.; Nwokeke, U.; Rodriguez, I.; Tirado, J. L. *Electrochem. Solid-State Lett.* **2008**, *11*, A209–A213.
(23) Kim, H.; Kim, Y. J.; Kim, D. G.; Sohn, H. J.; Kang, T. *Solid State Ionics* **2001**, *144*, 41–49.
(24) Larcher, D.; Beattie, S.; Morcrette, M.; Edstroem, K.; Jumas, J. C.; Tarascon, J. M. *J. Mater. Chem.* **2007**, *17*, 3759–3772.
(25) Idota, Y.; Kubota, T.; Matsufuji, A.; Maekawa, Y.; Miyasaka, T. *Science* **1997**, *276*, 1395–1397.